Viewing Zone Expansion of Autostereoscopic Display With Composite Lenticular Lens Array and Saddle Lens Array

Jian Zhao, Yiquan Ding, Ziyao Dai, Jie Gong, Guodong Tong, and Yinuo Zhang

***Abstract*—The light field display technology can reconstruct the virtual three-dimensional scene with high precision, providing users with a highly immersive viewing experience without any auxiliary equipment. However, one of the main challenges faced by this technology is the narrow field of view (FOV). In this paper, we present a novel autostereoscopic display utilizing Composite Lenticular Lens Array (CLLa) and Saddle Lens Array (SLa). By utilizing time-division quadruplexing, distinct contents are assigned to different pairs of viewing zones. The optical model of this scheme is simulated by ZEMAX. The FOV is expanded horizontally to 100 degrees and the crosstalk level is reduced to 0.8%, ideally. It is worth noting that both viewing zones share the same set of pixels, which theoretically results in a spatial resolution one times higher than traditional schemes. Furthermore, this scheme has been partially verified by a 7.9-inch TFT-LCD screen, and experimental results demonstrate an effective expansion of the field of view angle by more than 16.2% compared to traditional schemes.**

***Index Terms*—Light field display, field of view, micro-lens array.**

I. Introduction

THUS far, autostereoscopic display technology has a wide range of applications in various fields due to its considerable potential and benefits, including but not limited to car navigation, digital signage, biomedicine, military operations and education [1], [2], [3], [4]. For instance, medical professionals can readily execute 3D stereoscopic procedures without relying on 3D head-up displays in the realm of medical stereoscopic presentations [5]. In the realm of automotive navigation [6], autostereoscopic display systems can offer drivers an immersive navigation experience based on real-life scenarios. For educational purposes [7], students can visually experience the appearance and structure of 3D models. However, the existing naked-eye 3D display technology still faces the challenges such as insufficient spatial resolution, distorted depth perception, and limited field of view. greatly hinders the widespread adoption of this technology.

There are various technical solutions available for autostereoscopic display, such as holographic display [8], [9], volumetric 3D display [10], multi-layer liquid crystal display [11], [12], and light field display based on micro-lens arrays [13], [14]. Nevertheless, none of them can be deemed as the ultimate 3D display solution. Due to precise phase or amplitude modulation, holographic display technology [15] can reconstruct a 3D scene with ultra-high angular resolution within a specific viewing angle. Therefore, the user is able to observe almost all features of the real object at a specific location without visual fatigue. However, this technology suffers from speckle noise, narrow field of view, and large data volumes. The volumetric 3D display technology [16] could provide a seemingly continuous virtual scene by utilizing a high-speed variable-focus lens based on visual retention principles. Obviously, this technology is limited by its high refresh rate, power consumption, and large size. Multi-layer liquid crystal display [17] could render ultra-high spatial resolution of three-dimensional scene by controlling the light transmission rate of each layer of liquid crystal. This technology offers advantages such as thinness, low power consumption, and high spatial resolution. However, the depth-of-field is severely limited by the gap between liquid crystal layers. Light field display technology based on micro-lens array [18] is considered to be one of the best solutions for commercial autostereoscopic display due to its ability to provide high angular resolution and a large depth-of-field range without vergence-accommodation conflict (VAc) [19], [20]. However, the main challenges associated with this technology are narrow field-of-view and spatial resolution loss. In recent years, expanding the field-of-view of autostereoscopic displays has become a major area of research.

Several methods have been proposed to expand the field of view. A proposal was put forward for an autostereoscopic 3D display system featuring dynamic fusion of the viewing zone under eye tracking [21], which offers enhanced 3D image quality and an extended viewing range based on dynamic fusion of the viewing zone (DFVZ). A spatial reality display capable of autostereoscopic display [7] was proposed, utilizing Sony's

Manuscript received 14 June 2023; revised 25 July 2023; accepted 31 July 2023. Date of publication 3 August 2023; date of current version 15 August 2023. This work was supported in part by the National Natural Science Foundation of China under Grant 62075040 and in part by The Natural Science Foundation of the Jiangsu Higher Education Institutions of China under Grant 21KJB520038. *(Corresponding author: Jian Zhao.)*

Jian Zhao is with the School of Computer Engineering, Nanjing Institute of technology, Nanjing 211167, China, also with the School of Electronic Science and Engineering, Southeast University, Nanjing 210096, China, and also with the SuXin Vision Technologies Company Ltd, Suzhou 215000, China (e-mail: zhaojian@njit.edu.cn).

Yiquan Ding, Ziyao Dai, Jie Gong, and Yinuo Zhang are with the School of Computer Engineering, Nanjing Institute of technology, Nanjing 211167, China.

Guodong Tong is with the School of Electronic Science and Engineering, Southeast University, Nanjing 210096, China (e-mail: tongguodong@seu.edu.cn).

Digital Object Identifier 10.1109/JPHOT.2023.3301559

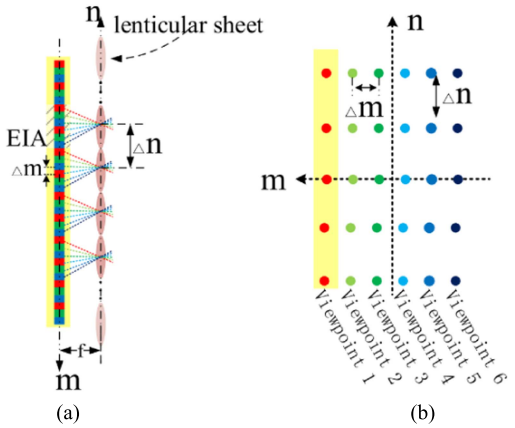

Fig. 1. Light space representation for autostereoscopic display. (a) Light field scan lines. (b) Two-dimensional sampling grid.

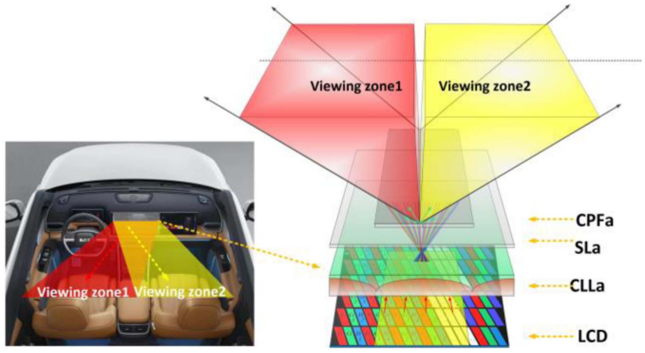

Fig. 2. Schematic diagram of structure principle.

high-speed vision sensor and face recognition technology to achieve accurate detection and eye recognition. Nonetheless, the occurrence of latency in dynamic response speed following a change in viewer position is an inevitable phenomenon. A light-field display system utilizing lenticular lens array (LLA), lens array (LA) and holographic functional screen (HFS) has been demonstrated [22]. The prototype achieved 70-degrees horizontal viewing angle and 30-degrees vertical viewing angle, with 11000 viewpoints obtained. However, the combination of a large field of view angle and dense viewpoints inevitably leads to spatial resolution loss. To address this issue, a projection-type integral imaging system [23] has been proposed to enhance the viewing zone of the input 3-D scene. However, the size has undergone a significant increase, while the spatial resolution has experienced a decrease.

In this article, a novel autostereoscopic display utilizing Composite Lenticular Lens Array (CLLa) and Saddle Lens Array (SLa) were proposed, which generates two symmetrical viewing zones within the field of view. By utilizing time-division quadruplexing, distinct contents are assigned to different pairs of viewing zones. Experimental results show that the field of view is expanded to 100 degrees, and the spatial resolution is doubled, theoretically.

II. Principle and Analysis

A. The Overall Design of the System

Currently, autostereoscopic display primarily relies on binocular parallax in the horizontal direction to produce stereo perception within the human brain. Therefore, the distribution of horizontal parallax will be emphasized in this article. As shown in Fig. 1(a), the lenticular sheet represents a continuous micro-lens array (MLa) in the horizontal direction with pitch of △n. The LCD layer's sub-pixel size is △m and is located on the back focal plane of the lenticular, with a gap equal to the focal length f of the lenticular. The n-axis defines the plane of the lenticular, while the m-axis defines that of the LCD screen. It should be noted that the two axes are oriented in opposite directions. In conventional integrated imaging, the subpixel region is defined as the elemental image array (EIa) covered by a single lenticular. However, the inconsistent relative distances between each subpixel and the lenticular optical axis result in directional refraction of light propagation after passing through the lenticular. Therefore, the subpixel density in EIa can reflect the angular resolution of integrated imaging, while the width of the micro-lens can reflect the spatial resolution. The field of view can be defined as the maximum spatial angle of refracted light from the two sides of EIa subpixels after passing through their corresponding lenticular, as expressed in (1) [24],

$$\theta = \arctan \frac{\Delta \mathrm{n}}{2f} \tag{1}$$

Cartesian coordinate system (m, n) is established, where the m-axis denotes the LCD layer and the n-axis represents the lenticular sheet, as illustrated in Fig. 1(b). Each point on the figure corresponds to a light ray emitted from sub-pixel m and passing through lenticular n. The interval of each column represents the sub-pixel interval, also known as viewpoint interval or angular resolution (△m), while the interval of each row represents the lens section width, also known as spatial resolution (△n). According to (1), △m is a constant for a specific display device. To expand the field of view, one can achieve this by increasing the pitch △n or decreasing the focal length of the lens. Expanding the field of view by increasing the pitch of lenticular result in a reduction of spatial resolution and a significant increase in granularity sensation. To further explore the reduction of focal length, if the interval between the LCD and the column lens array is g, the focal length of the lenticular is f, and the depth of field of the integrated imaging system can be derived as d, as shown in (2):

$$\mathrm{d} = \frac{f\mathrm{g}}{f+g} \tag{2}$$

According to (2), as the focal length f decreases, the system depth of field d also decreases. Therefore, attempting to expand the field of view by increasing pitch △n or decreasing focal length f will lead to a reduction in spatial resolution and depth of field.

Considering the above problems, the principle of the novel autostereoscopic display is illustrated in Fig. 2. The system is composed of an LCD layer, Composite Lenticular Lens Array

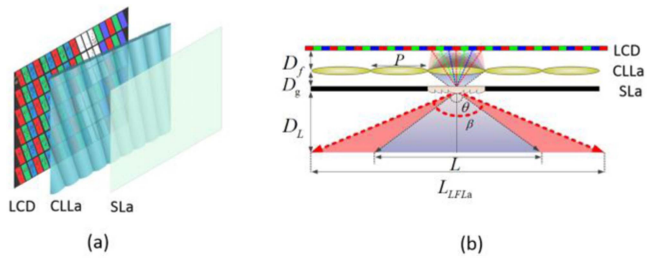

Fig. 3. (a) Structure diagram of the proposed system. (b) Top view.

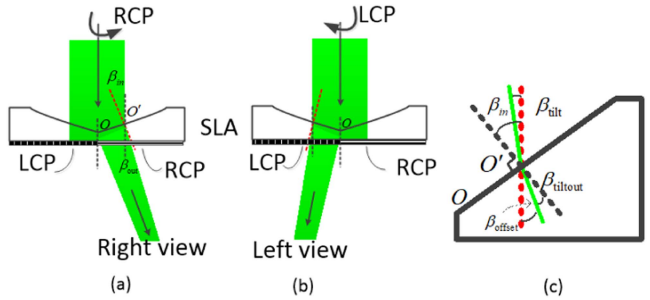

Fig. 4. (a) Right view based on RCP. (b) Left view based on LCP. (c) Schematic diagram of right-trapezoid refraction.

(CLLa), Saddle Lens Array (SLa), and Circular Polarization Filter array (CPFa) layer. By utilizing time-division quadruplexing, the backlight source is converted into left-handed and right-handed circularly polarized light. Subsequently passing through SLa and CPFa, the system is capable of generating viewing zone 1 and viewing zone 2. The two independent viewing zone can display either two completely different contents or a large FOV light field content with continuous parallax, and the specific display principle is described in the next section.

To mitigate the impact of moiré, a conventional approach is to rotate CLLa along the optical axis by an angle [25]. However, this also presents an additional challenge: luminance leakage between pixels, leading to cross-talk issues from different viewpoints. In our previous work [26], a tilted pixel design solution was proposed and it is experimentally demonstrated that the scheme can effectively suppress channel crosstalk. Therefore, the autostereoscopic display will also mitigate the moiré effect based on this structural, as shown in Fig. 3(a). The pitch of CLLa is designated as P, while the focal length and light viewing distance are respectively denoted by D_g and D_L. Additionally, the field of view without SLa is represented by θ and that with SLa represented by β. The interval D_f between the LCD and CLLa need to be strictly equal to the back focal length of CLLa.

B. Viewing Zone Expansion

SLa is a saddle-shaped concave lens composed of two right-trapezoid lenses with center point O, as shown in Fig. 4. The left-hand circular polarizer and the right-hand circular polarizer are positioned beneath the longer sides of their right-trapezoid lenses, respectively. The circular polarizer has the same dimensions as those of right-trapezoid lenses. Since the incident light is

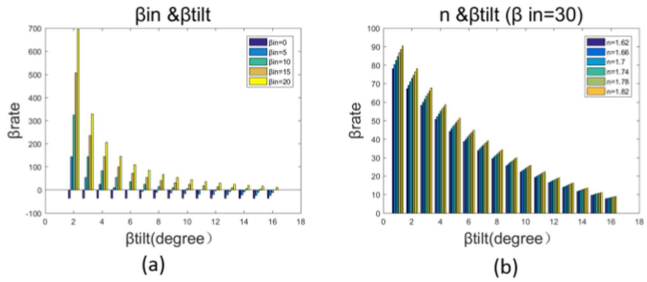

Fig. 5. (a) The impact of β_{in} and β_{tilt} on β_{rate} with a refractive index n = 1.56. (b) The impact of refractive index and β_{tilt} on β_{rate} with $\beta_{\text{in}} = 30$.

a parallel beam, it will have a certain intersection area with SLa. The rightmost point of contact between the incident light and SLa is assumed to be O'. When the beam is incident vertically, the angle of incidence is β_{in}. According to the principle of light refraction, the angle of refraction β_{out} can be determined,

$$\beta_{\text{out}} = \arcsin\left(\frac{\sin\beta_{\text{in}}}{n}\right) \tag{3}$$

where n is the refractive index. It is worth noting that the angle of incidence β_{in} is equivalent to the slope of a right-trapezoid. It can be seen that the incident light is split into two beams with different polarization states on the left and right after passing through the SLa. If the polarization state of the incident light is right-handed circularly polarized, only the right-handed circularly polarized film can transmit the refracted light to form a right view, as illustrated in Fig. 4(a). Conversely, the left-handed circularly polarized film can transmit the refracted light to form a left view, as shown in Fig. 4(b).

When the angle of inclination is denoted as β_{tilt}, as shown by the green line in Fig. 4(c), the actual angle of incidence β_{tiltin} is:

$$\beta_{\text{tiltin}} = \beta_{\text{in}} - \beta_{\text{tilt}} \tag{4}$$

The angle of refraction β_{tiltout} is:

$$\beta_{\text{tiltout}} = \arcsin\left(\frac{\sin\beta_{\text{tiltin}}}{n}\right) = \arcsin\left(\frac{\sin(\beta_{\text{in}} - \beta_{\text{tilt}})}{n}\right) \tag{5}$$

The offset of light propagation direction β_{offset} can be obtained:

$$\beta_{\text{offset}} = \beta_{\text{in}} - \beta_{\text{tiltout}} = \beta_{\text{in}} - \arcsin\left(\frac{\sin(\beta_{\text{in}} - \beta_{\text{tilt}})}{n}\right) \tag{6}$$

Therefore, the FOV expansion ratio β_{rate} is:

$$\begin{aligned}\beta_{\text{rate}} &= \frac{2 * \beta_{\text{offset}} - 2 * \beta_{\text{tilt}}}{2 * \beta_{\text{tilt}}} \\ &= \frac{\beta_{\text{in}} - \beta_{\text{tilt}} - \arcsin\left(\frac{\sin(\beta_{\text{in}} - \beta_{\text{tilt}})}{n}\right)}{\beta_{\text{tilt}}} * 100\%\end{aligned} \tag{7}$$

As shown in (7), the FOV expansion ratio is related to the refractive index n and the reference β_{in}.

In Fig. 5(a), it can be observed that when the refractive index n is 1.56, an increase in β_{tilt} for a fixed β_{in} results in a decrease

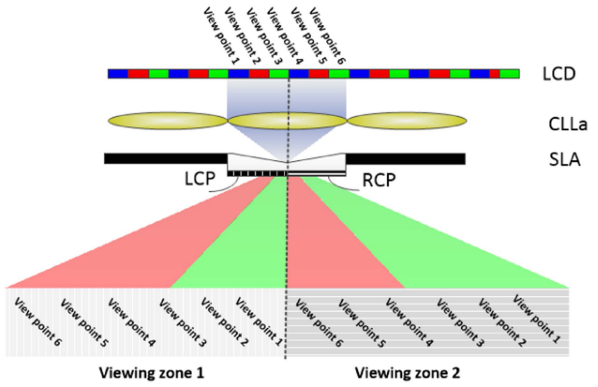

Fig. 6. Schematic diagram of partition display.

in the expansion ratio β_{rate}. When β_{tilt} is a fixed value, an increase in β_{in} results in a higher expansion ratio β_{rate}. It means that the larger the slope of the right-trapezoid lens is, the higher the expansion ratio will be. It is worth noting that the expansion ratio is negative when β_{in} is smaller than β_{tilt}. The physical significance is that when the incident light enters the first quadrant of the Cartesian coordinate system defined by normal line and slope, according to the light refraction theorem, the refracted light will also be shifted to the third quadrant. At this point, the field of view will be compressed. When β_{in} is 30°, the refractive index n is positively correlated with the expansion ratio, as shown in Fig. 5(b). Its physical meaning is that the refractive index of a lens reflects its ability to manipulate light. In addition, the expansion ratio is inversely proportional to β_{tilt} for a given refractive index n and β_{in}, ensuring that the newly generated viewpoints are evenly spaced and continuous in space.

C. Partitioning Display

As described in the previous section, the incident light is split into two beams with different polarization states on the left and right after passing through the SLa, as the red or green area shown in Fig. 6. when the polarization state of the incident light is right-handed circularly polarized, only the right-handed circularly polarized film can transmit the refracted light to form a right view. Assuming that there are only six viewpoints in EIa, light field 2 with six viewpoints is reconstructed in viewing zone 2. Similarly, if the incident light is left-handed circularly polarized, light field 1 is reconstructed in viewing zone 1. However, light field 1 and light field 2 are identical and share a common set of subpixels due to the same EIa. By utilizing time-division quadruplexing, the LCD displays EIa1 and EIa2 with different contents. Light field 1 and light field 2 are reconstructed by EIa 1 and EIa 2, respectively. In this case, the viewing zone is enlarged in the horizontal direction, which enables two viewers to have specific views corresponding to the positions of their own eyes without interfering with each other's view. If the LCD displays EIa1 and EIa2 with continuous parallax, a super large FOV of light field can be obtained. It is worth noting that all of this is based on a set of EIa sub-pixels, so the display resolution is double that of traditional methods.

TABLE I
PARAMETERS OF SIMULATION MODEL

Parameters	Values
Resolution of LCD panel	1536(w)xRGBx2048(H)
Pixel Pitch	0.026mm x 0.078mm
Pitch of the lenticular lens (P)	1. 74 mm
Index of refraction	1.76 and 1.51
Thickness of CLLa	2.5mm and 0.5mm
The focal length of CLLa (Df)	0.9 mm
Pitch of SLa	1. 74 mm
Thickness of SLa	0.1 mm
+Depth/-Frequency of SLa	0.5
The gap between CLLa and LCD	0.9mm
The gap between SLa and LCD	3.9mm
Resolution of CCD	1100 x 1100
Size of CCD	866 x 866 mm
The distance between CCD and LCD	500mm

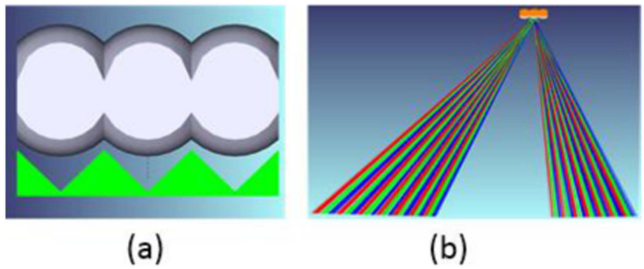

Fig. 7. Simulation model. (a) Sectional view. (b) Top view.

III. SIMULATION AND EXPERIMENTS

A. Simulation Results

To validate our concept, we conducted a simulation model to showcase the proposed design discussed earlier. Our optical setup adheres to the layout illustrated in the simulation model, with a sub-pixel size of 0.026 mm (W) × 0.078 mm (H). The CLLa has a section width of 1.74 mm and refractive indices of 1.76 and 1.51 respectively, while the SLa section width matches that of CLLa at 0.1 mm thickness. This simulated optical model was established by ZEMAX and SLa can be done by Fresnel lenses, because the Lenticular Fresnel lens achieves the same optical effect by dividing the Lenticular lens out into a series of Fresnel bands. In fact, a Fresnel lens can be regarded as a series of prisms arranged according to certain rules. The aspheric formula for a Fresnel lens is:

$$z = \frac{cr^2}{1+\sqrt{1-(1+k)c^2r^2}} + a_2r^2 + a_4r^4 + a_6r^6 \ldots \quad (8)$$

Where c represents the vertex curvature, r denotes the radial coordinate, k stands for the conic constant, and a2, a4, and a6 are aspheric coefficients. The optical parameters are presented in Table I:

The simulation results presented in Fig. 7(a) demonstrate CLLa as the gray component and SLa as the green component. The RGB sub-pixels are represented by beams of different colors. Additionally, in order to better evaluate the partitioning

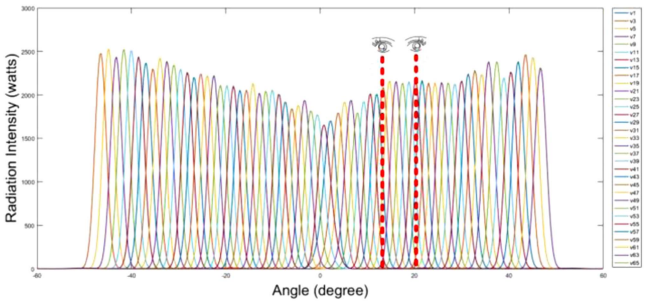

Fig. 8. Light intensity distribution of partial viewpoints.

TABLE II
THE PARAMETERS OF THE EXPERIMENT

Parameters	Values
Diagonal size	7.9" Landscape
Resolution of LCD panel	1536(w)xRGBx2048(H)
Pixel Pitch	0.026mm (W) x 0.078mm (H)
Glass Thickness (D_f)	0.9mm
Pitch of CLLa (P)	1.74mm
The focal length of CLLa (D_f)	0.9mm
Pitch of SLa	1.74mm
Viewpoint number	68
Component Angle	9.46°
Display depth	300mm

effect, certain pixels have been illuminated. Those viewpoints located on the right side of the optical axis are illuminated with red, green, and blue color. The Fig. 7(b) shows that both sets of beams are composed of quasi-parallel beams arranged in a specific order, as indicated by their respective colors. This verifies the light field partitioning display proposed in the Section II-C.

To assess the light field modulation capability of the proposed method, we simulated the luminance of partial viewpoints at the target location and present the results in Fig. 8. The distribution of light intensity is weakened in the middle due to SLa, but stronger on both sides. Nevertheless, this discrepancy is not significant and can be compensated for by the LCD's own light intensity distribution. According to the calculation, when the interpupillary interval is 60mm, the angle of vergence is 6.9 degrees relative to the screen. According to this parameter, the span of viewpoints is 12 and the crosstalk level is 0.8% between the left and right eyes, ideally.

B. Experimental Results

In order to further verify the ability of the proposed scheme to expand the field of view in horizontal direction, this experimental part uses the display module IG079, which is 7.9- inch LCD panel (Thin Film Transistor Liquid Crystal Display) module composed of LCD panel. The LCD panel produces a higher resolution image that is composed of 1536 × 2048 pixel elements in a stripe arrangement. In order to verify the proposed optical system, the parameters of this experiment are listed in Table II. The refresh rate of the scheme is 60 Hz, and the commonly used

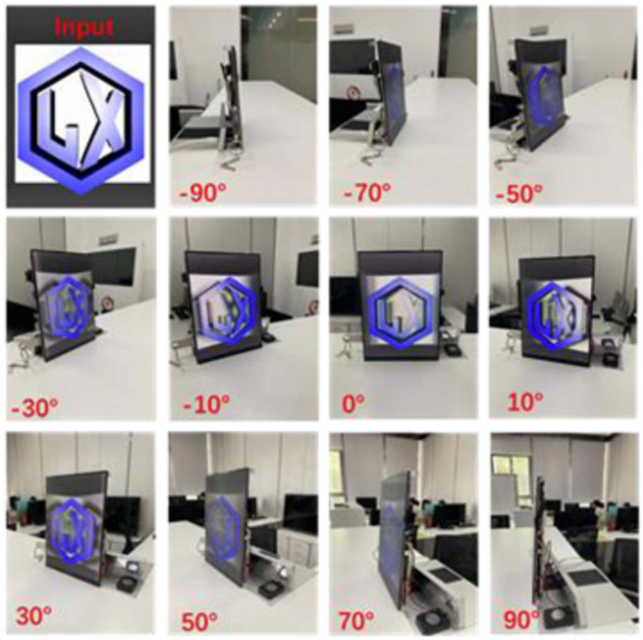

Fig. 9. Photographs of the reconstructed object taken horizontally.

commercial displays can meet the requirements, and there is no increase in technical difficulty and cost.

According to the analysis in the Section II-C, the partitioned display is feasible in principle. It is worth stating that there is currently no polarization source available based on time-division multiplexing, SLa is not incorporated in the experimental part. Instead, the experimental results were obtained by independent collection of two viewing zones. By displaying two sets of continuous parallax sequence images for the left and right viewing zones respectively, the results are collected at different positions. This scheme can be equivalent to verify the conclusions of Part 2.3. In this experiment, there are a total of 68 viewpoints and the parallax increases in a sequential manner. When capturing the viewing zone 1, the LCD screen displays viewpoints ranging from 1 to 33. Similarly, when the viewing zone 2 is photographed, the LCD display is refreshed and shows viewpoints ranging from 34 to 66. The results are shown in Fig. 7. As depicted in Fig. 9(a), the input model is presented. The display quality experiences a notable decline within the range of 70 to 90 degrees in both viewing zones. In the range of 50 to 70 degrees, the display quality is significantly improved, but the display is flat. Therefore, this part is called the invalid autostereoscopic display area. However, within the range of −50 to +50 degrees, a 3D reconstruction object with a strong sense of immersion is captured. The measured field of view angle exceeds 100 degrees. According to (1), the field of view is 86 degrees without SLa. Therefore, the experimental results validate that this solution can effectively expand FOV by over 16.2%. Additionally, it enables independent display of dual viewing areas (in the case of time-division multiplexed polarized light sources) and the spatial resolution is doubled, theoretically. As the light source is circularly polarized, the two viewing zones operate independently under the state of time multiplexing. The

advantage of this is that the crosstalk between the viewing zone is almost zero.

IV. Conclusion

To tackle the issue of limited field of view in light field display, a novel autostereoscopic display utilizing Composite Lenticular Lens array (CLLa) and Saddle Lens array (SLa) has been proposed, which generates two symmetrical viewing zones within the field of view. A 7.9-inch LCD panel with a pixel density of 324 PPI was utilized in this experiment. The results indicate that the field of view (FOV) can be expanded by 16.2%, crosstalk level is reduced to 0.8%, and spatial resolution is doubled without increasing lens width or reducing focal length, ideally. This technology has potential applications in smart cockpits with partitioned displays, medical surgeries and monitoring, and computer gaming.

References

[1] J. Hua et al., "Foveated glasses-free 3D display with ultrawide field of view via a large-scale 2D-metagrating complex," *Light Sci. Appl.*, vol. 10, no. 1, 2021, Art. no. 213.

[2] G. Chen et al., "A naked eye 3D display and interaction system for medical education and training," *J. Biomed. Inform.*, vol. 100, 2019, Art. no. 103319.

[3] Y. He et al., "Harnessing the plenoptic function for a directionally illuminated autostereoscopic display," *Opt. Exp.*, vol. 30, no. 25, pp. 45553–45568, 2022.

[4] J. C. A. Read et al., "Viewing 3D TV over two months produces no discernible effects on balance, coordination or eyesight," *Ergonomics*, vol. 59, no. 8, pp. 1073–1088, 2016.

[5] Y. Zhao, Y. Wei, X. Cui, L. Qu, L. Liu, and Y. Wang, "3D display technology in medical imaging field," in *Proc. IEEE Int. Conf. Med. Imag. Phys. Eng.*, 2013, pp. 210–214.

[6] J. Skirnewskaja and T. D. Wilkinson, "Automotive holographic head-up displays," *Adv. Mater.*, vol. 34, no. 19, 2022, Art. no. e2110463.

[7] T. Itamiya et al., "A novel anatomy education method using a spatial reality display capable of stereoscopic imaging with the naked eye," *Appl. Sci.*, vol. 11, no. 16, 2021, Art. no. 7323.

[8] M. Park et al., "360-degree mixed reality volumetric display using an asymmetric diffusive holographic optical element," *Opt. Exp.*, vol. 30, no. 26, pp. 47375–47387, 2022.

[9] S. Choi et al., "High-quality holographic displays using double SLMs and camera-in-the-loop optimization," *Proc. SPIE*, vol. 11765, pp. 171–178, 2021.

[10] C. Martinez et al., "Multi-user volumetric 360 degrees display based on retro-reflective transparent surfaces," *Opt. Exp.*, vol. 28, no. 26, pp. 39524–39543, 2020.

[11] D. Kim et al., "Hybrid multi-layer displays providing accommodation cues," *Opt. Exp.*, vol. 26, no. 13, pp. 17170–17184, 2018.

[12] D. Lanman et al., "Polarization fields: Dynamic light field display using multi-layer LCDs," *Assoc. Comput. Machinery Trans. Graph.*, vol. 30, pp. 1–10, 2011.

[13] R. Li et al., "Compact integral imaging 2D/3D compatible display based on liquid crystal micro-lens array," *Liquid Crystals*, vol. 49, no. 4, pp. 512–522, 2021.

[14] X. L. Ma et al., "Depth of field and resolution-enhanced integral imaging display system," *Opt. Exp.*, vol. 30, no. 25, pp. 44580–44593, 2022.

[15] C. Chang et al., "Toward the next-generation VR/AR optics: A review of holographic near-eye displays from a human-centric perspective," *Optica*, vol. 7, no. 11, pp. 1563–1578, 2020.

[16] K. Suzuki, Y. Fukano, and H. Oku, "1000-volume/s high-speed volumetric display for high-speed HMD," *Opt. Exp.*, vol. 28, no. 20, pp. 29455–29468, 2020.

[17] L. Zhu et al., "Performance improvement for compressive light field display based on the depth distribution feature," *Opt. Exp.*, vol. 29, no. 14, pp. 22403–22416, 2021.

[18] L. Liu et al., "Depth of field analysis for a three-dimensional light-field display based on a lens array and a holographic function screen," *Opt. Commun.*, vol. 493, 2021, Art. no. 127032.

[19] Q. Sun et al., "Eccentricity effects on blur and depth perception," *Opt. Exp.*, vol. 28, no. 5, pp. 6734–6739, 2020.

[20] Y. Watanabe and H. Kakeya, "Time-division and color multiplexing light-field display using liquid-crystal display panels to induce focal accommodation," *Appl. Opt.*, vol. 60, no. 7, pp. 1966–1972, 2021.

[21] K. H. Yoon et al., "Autostereoscopic 3D display system with dynamic fusion of the viewing zone under eye tracking: Principles, setup, and evaluation," *Appl. Opt.*, vol. 57, no. 1, pp. A101–A117, 2018.

[22] Y. Wang et al., "Three-dimensional light-field display with enhanced horizontal viewing angle by introducing a new lenticular lens array," *Opt. Commun.*, vol. 477, 2020, Art. no. 126327.

[23] H. Watanabe et al., "Pixel-density and viewing-angle enhanced integral 3D display with parallel projection of multiple UHD elemental images," *Opt. Exp.*, vol. 28, no. 17, pp. 24731–24746, 2020.

[24] J. Zhao and J. Xia, "Virtual viewpoints reconstruction via Fourier slice transformation," *J. Soc. Inf. Display*, vol. 26, no. 8, pp. 463–469, 2018.

[25] C. C. Ji et al., "Tilted elemental image array generation method for moire-reduced computer generated integral imaging display," *Opt. Exp.*, vol. 21, no. 17, pp. 19816–19824, 2013.

[26] Q. Ma, J. Zhao, S. Zhang, L. Yuan, J. Xia, and J. Wu, "Tilted LCD pixel with liquid crystal GRIN lens for two-dimensional/three-dimensional switchable display," *IEEE Photon. J.*, vol. 11, no. 4, Aug. 2019, Art. no. 6901509.